Laser-frequency mixing in a scanning tunneling microscope at 1.3 μm

Th. Gutjahr-Löser,[a] A. Hornsteiner,[b] W. Krieger,[c] and H. Walther
Max-Planck-Institut für Quantenoptik, Hans-Kopfermann-Str. 1, D-85748 Garching, Germany

(Received 10 November 1998; accepted for publication 2 February 1999)

The radiation of two single-mode diode lasers at 1.3 μm is focused into the tunneling junction of a scanning tunneling microscope, and gigahertz difference-frequency signals radiated from the tip are detected. Simultaneous measurements of the bias-voltage dependence of the mixing signal and the tunneling current for different surface samples show that the mixing process is due to the nonlinearity of the static current–voltage characteristic of the tunneling junction. The coupling of the laser radiation into the junction conforms to antenna theory. The experimental results are compared with previous measurements at a laser wavelength of 9.3 μm. Surface images produced by means of the difference-frequency signal show the chemical contrast between micron-sized Au islands and a graphite substrate. © *1999 American Institute of Physics.* [S0021-8979(99)08109-8]

INTRODUCTION

When electromagnetic radiation is coupled into the scanning tunneling microscope (STM), the tunneling junction acts as a nonlinear mixer generating harmonics, difference frequencies, and rectified currents. These nonlinear signals lead to some interesting additional applications of the STM, such as imaging of insulating surfaces,[1] generation of new surface images with atomic resolution,[2] realization of a laser-driven STM,[3] and detection of surface plasmons[4] and surface acoustic waves.[5] Many of these experiments aim at development of locally resolved spectroscopy of surface resonances. This requires access to a broad spectral range from microwaves to the visible spectral region.

Generation of nonlinear signals was previously observed with microwaves (second- and third-harmonic generation)[1,6–8] and with infrared light at 9.3 μm (difference-frequency generation and rectification).[9] In the visible spectral range, only rectification has hitherto been observed.[1,10,11] Recent theoretical simulations predict a strong increase of the laser-induced components of the tunneling current when the wavelength is decreased from the infrared to the visible spectral range, and resonance behavior in the ultraviolet.[12] Experiments at shorter wavelengths are therefore desirable.

In this contribution we investigate the generation of gigahertz difference-frequency signals in the STM by using the radiation of two diode lasers at 1.3 μm, thus bridging the gap between 9.3 μm and the visible spectral range. The use of diode lasers has the advantage of providing access to a continuous range of difference frequencies throughout the microwave region.

The experiments prove that difference-frequency generation, also at 1.3 μm, is determined by the nonlinearity of the static current–voltage ($I-V$) characteristic of the tunneling junction. The coupling of the radiation into the junction conforms to antenna theory. This model is used to explain the considerable decrease of the mixing signal from 9.3 to 1.3 μm. In a first application, the possibility of distinguishing micron-sized Au islands from the graphite substrate is demonstrated by using images obtained with the difference-frequency signal.

EXPERIMENTAL SETUP

The experimental setup consists of the diode-laser system, the STM, and the microwave-detection system. A schematic drawing of the laser system is shown in Fig. 1. The beams of two diode lasers are superimposed and amplified by a third diode. All three lasers (Oki OL303A-20) with an emission wavelength of 1.3 μm are antireflection-coated on their output facets with a reflectivity of less than 10^{-4}. Lasers 1 and 2 have external cavities consisting of a grating and a mirror in the Littman configuration in order to achieve single-mode operation.[13,14] This configuration allows wavelength tuning without displacing the output beam. The maximum single-mode output power of each laser is 6 mW.

In our experiment the stability of the difference frequency between the two lasers is crucial. To maintain a constant difference frequency we employ a feedback system acting on laser 2. The difference frequency is measured with a fast photodiode. In a first step the photodiode output is mixed with a reference signal from a microwave synthesizer, resulting in an intermediate frequency of 200 MHz. In a second mixer this frequency is compared with a reference frequency from a quartz oscillator. The mixer output directly modulates the driving current of diode laser 2 (phase-locked loop). The slow components of the mixer signal are used to tilt the laser mirror with a piezo drive in order to compensate for slow fluctuations. A similar feedback loop was recently reported.[15]

The feedback circuit reduces the linewidth of the difference-frequency signal from about 100 kHz to less than 30 Hz (the minimum bandwidth of the spectrum analyzer

[a]Present address: Max-Planck-Institut für Mikrostrukturphysik, Weinberg 2, D-06120 Halle, Germany.
[b]Present address: Laser 2000 GmbH, Argelsrieder Feld 14, D-82234 Wessling, Germany.
[c]Electronic mail: wgk@mpq.mpg.de

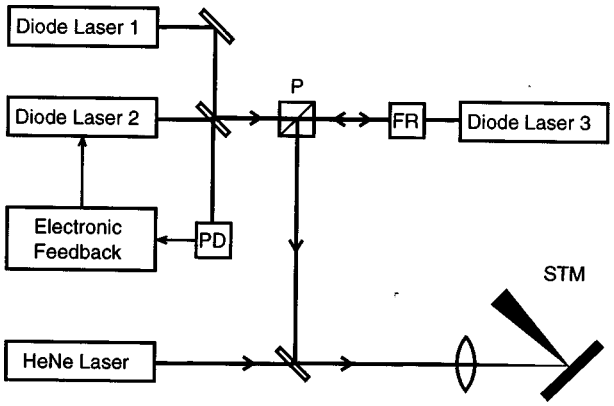

FIG. 1. Schematic drawing of the experimental setup (P=polarizing beam splitter, PD=photodiode, FR=Faraday rotator).

used for the measurements). The difference frequency can be varied from 30 MHz to 10 GHz. The upper limit is set at present by the bandwidth of the photodiode used for the experiments.

In order to increase the output power, the superimposed beams are amplified by a third diode laser without grating. As shown in Fig. 1, the amplifying diode laser is used in the reflection geometry. The output beam is separated from the input beam by a Faraday rotator in conjunction with a polarizing beam splitter. By comparing the magnitude of the beat signals before and after amplification it was verified that the two beams were equally amplified. To protect diode laser 3 from possible damage, the system was operated with an output power not exceeding 20 mW.

The beam is focused into the tunneling junction of the STM by means of a microscope objective with a focal length of 25 mm. The diameter of the focus is 15 μm. Its position is controlled with a motorized xyz-translation stage. Adjustment is done with the help of a visible tracer beam from a He–Ne laser. In order to keep the laser focus fixed on the tip while the image is being recorded, the sample is scanned

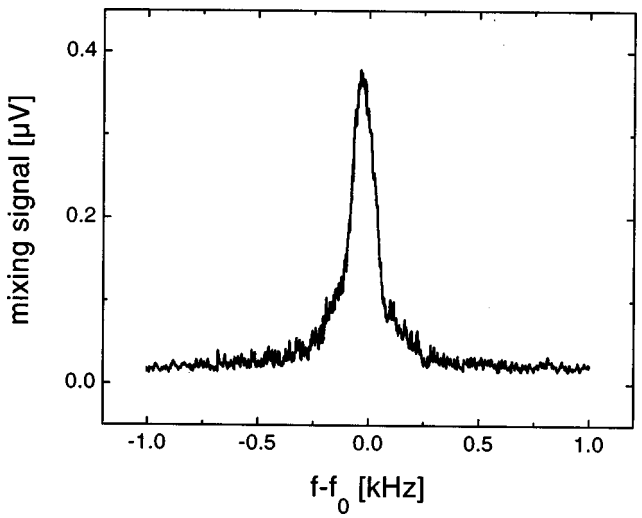

FIG. 2. Spectrum of the difference-frequency signal obtained from the STM on a Au surface. The center frequency f_0 is 6.9 GHz. The resolution bandwidth of the spectrum analyzer is 100 Hz.

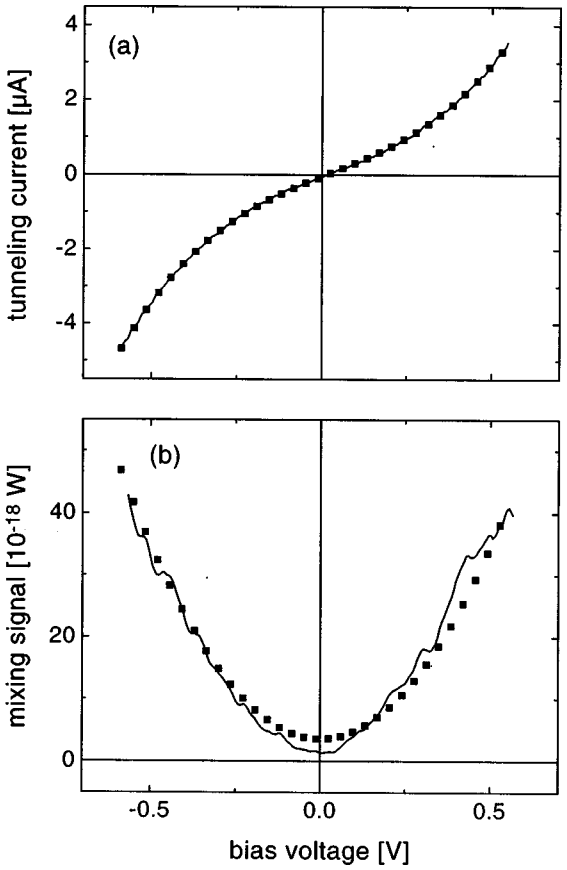

FIG. 3. Bias dependence of (a) the tunneling current and (b) the difference-frequency signal for a Au sample (tunneling parameters: $V_b=-600$ mV, $I=-4.7$ μA; total laser power $P=18$ mW). The dotted curves are fits as described in the text.

with a piezo tube. Commercial Pt/Ir tips were used in the STM. The samples investigated were 50-nm-thick Au and Ag layers, evaporated on glass substrates, and highly oriented pyrolytic graphite (HOPG). A pattern of micron-sized gold islands was prepared on a HOPG substrate by evaporating Au through two fine grids, slightly rotated with respect to each other to form a Moiré pattern.[16] The island size obtained varied between 1 and 30 μm. The HOPG sample was freshly cleaved before each experiment. To reduce contamination the Au and Ag samples were kept under vacuum before usage. STM images of the metal samples showed the grainy structure typical for evaporated films. No crystalline ordering was apparent.

The difference-frequency signals radiated by the tip are collected with an open waveguide mounted close to the STM. After amplification (40 dB) with a low-noise amplifier, the frequency of the signal is down converted to 200 MHz in a microwave mixer. The signal is again amplified (65 dB) and finally detected by means of a spectrum analyzer. This heterodyne detection technique has the advantage of making resolution bandwidths as small as 100 Hz possible at the low detection frequency. The noise level of the detection system at a bandwidth of 100 Hz is -142 dBm (6×10^{-18} W), which is close to the thermal noise level of -148 dBm at room temperature. For all experiments the tunneling junction was kept under normal pressure conditions in the laboratory.

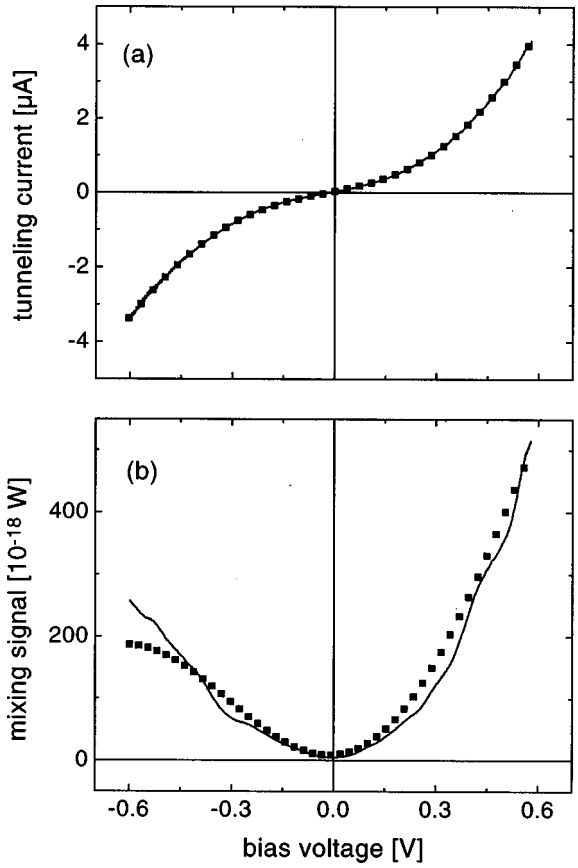

FIG. 4. Bias dependence of (a) the tunneling current and (b) the difference-frequency signal for a Ag sample (tunneling parameters: $V_b = 600$ mV, $I = 4$ μA; total laser power $P = 18$ mW). The dotted curves are fits as described in the text.

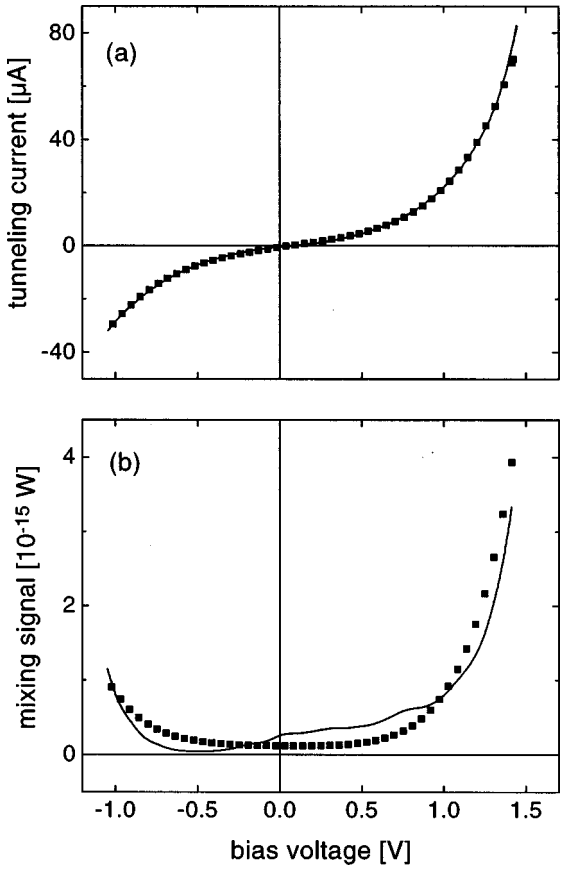

FIG. 5. Bias dependence of (a) the tunneling current and (b) the difference-frequency signal for a graphite sample (tunneling parameters: $V_b = -300$ mV, $I = -3$ μA; total laser power $P = 14$ mW). The dotted curves are fits as described in the text.

RESULTS

The frequency-mixing experiments were carried out at difference frequencies near 7 GHz with laser powers between 14 and 20 mW focused into the tunneling junction. This corresponds to intensities between 8 and 11 kW/cm^2.

The power of the difference-frequency signals was found to be strongly dependent on the shape of the tips. Signals were only detected if the diameter of the first few microns of the tips was of the order of the laser wavelength $\lambda = 1.3$ μm or smaller. The tips were individually selected for the experiments using images obtained with a scanning electron microscope. Optimal tips had a cone angle of less than 10°. The cone diameter then remains smaller than λ over a distance of at least 5λ from the tip.

The difference-frequency signal was observed to be dependent on the polarization direction of the incident laser light. Maximum signals were recorded when this direction was in the plane defined by the tip axis and the laser beam. At perpendicular polarization the signals were reduced by 5 dB.

Figure 2 shows a spectrum of the difference-frequency signal as obtained with a gold surface using a total incident laser power of 14 mW. The center frequency is $f_0 = 6.9$ GHz, and the signal width in this example is limited by the bandwidth of the spectrum analyzer of 100 Hz. The tunneling parameters are: bias voltage 500 mV, tunneling current 5 μA. The power of the difference-frequency signals observed with Au and Ag samples was typically 10^{-17} W. On HOPG samples, the difference-frequency signals were one order of magnitude smaller.

Since the difference-frequency signals were observed to grow with the tunneling current, their generation was as-

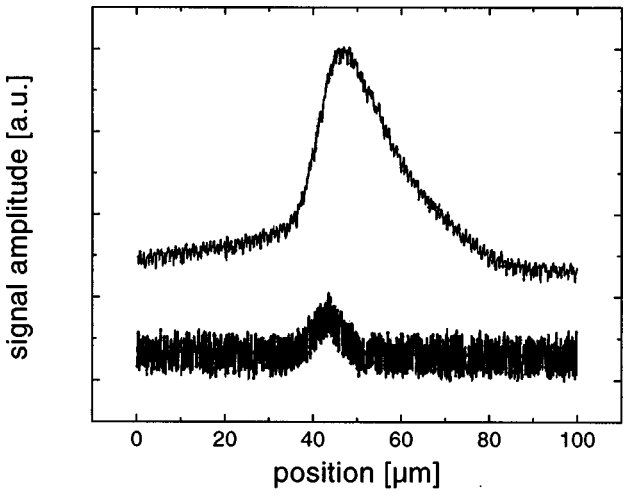

FIG. 6. Laser-induced dc current (upper curve) and difference-frequency signal (below) as a function of the focus position along the tip axis.

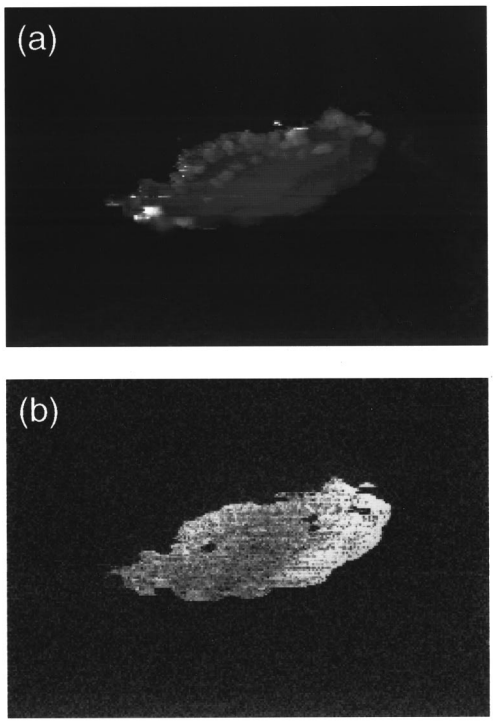

FIG. 7. (a) Topography and (b) difference-frequency signal of Au island on HOPG. Image size: 8.5 μm×6 μm.

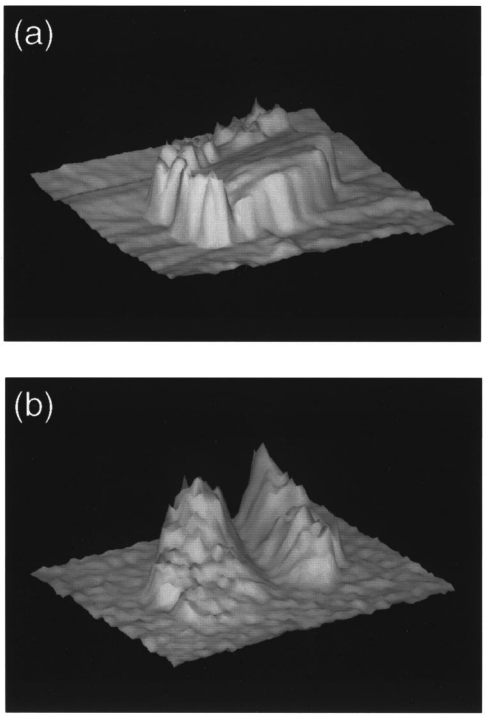

FIG. 8. (a) Topography and (b) difference-frequency signal of Au island on HOPG. Image size: 8.5 μm×6.5 μm.

sumed to be connected with the nonlinearity of the $I-V$ characteristics of the tunneling junction. In order to test this hypothesis, the bias-voltage dependence of the tunneling current and of the power of the difference-frequency signal were recorded simultaneously. For this measurement the distance control of the STM was periodically interrupted for 200 ms. During this interval a voltage ramp was applied to the tip, and the tunneling current and the power of the difference-frequency signal were recorded. The results of such measurements for samples of Au, Ag, and HOPG are shown in Figs. 3, 4, and 5, respectively. The curves in the figures are averages over 30 single measurements. Fluctuations in the signals are ascribed to lateral drifts of the tip position and to changes of the tip–sample distance during the voltage scans.

Besides a difference-frequency signal, a laser-induced direct current (dc) is also generated in the tunneling junction. In order to distinguish this current from the normal bias-induced tunneling current, it was measured at zero bias voltage. For this purpose the bias voltage was disconnected for 0.5 ms every 25 ms and the distance control was simultaneously disabled. The laser-induced dc current was measured during this period by means of a boxcar integrator.

Figure 6 shows a simultaneous measurement of the laser-induced dc current (upper curve) and the difference-frequency signal (below) as the laser focus is moved along the tip axis. The sample is HOPG. A mixing signal is only observed when the laser focus is located on the tunneling junction. The width of the signal corresponds to the focus diameter of 15 μm. The laser-induced dc current, however, shows a much wider distribution. A dc current is still observable when the laser focus is moved more than 30 μm from the tunneling junction.

Difference-frequency generation in the STM can be used to distinguish different materials at the sample surface, i.e., detect chemical contrast. To demonstrate this possibility the pattern of Au islands on HOPG was used. Images of the topography and the difference-frequency signal, simultaneously recorded over two such islands, are shown in Figs. 7 and 8. The image sizes are 8.5 μm×6.5 μm and 8.5 μm× 6 μm, respectively. The height of the islands is ≈50 nm. The bias voltages applied were 100 mV for Fig. 7 and 20 mV for Fig. 8. Both images were obtained with a total laser power of 17 mW at a difference frequency of 6.8 GHz. A mixing signal is only detected on the Au islands. No signal above the noise level of 6×10^{-18} W is observed on the bare HOPG substrate. The maximum signal on the islands corresponds to 3×10^{-17} W. As seen in Fig. 7, the rise of the difference-frequency signal closely follows the topographical edge of the island. The topographical features on top of the island, however, do not find any correspondence in the mixing signal image. Similarly the small ''holes'' in the mixing signal on the island cannot be correlated with any visible topographical structures. This behavior is strikingly demonstrated with a different island in Fig. 8 which is divided by a deep valley, when imaged with the difference-frequency signal.

DISCUSSION

The nonlinear response of the tunneling junction of the STM to laser radiation can be understood from a model consisting of two parts: a description of the coupling of the radiation into the junction, and of the generation of the nonlinear current components.[17]

The coupling is modeled either by using antenna theory (in the infrared spectral range)[17] or by excitation of surface plasmons localized between the tip and sample with resonances in the visible spectral range.[18] Different angular dependences of the coupling efficiency are predicted for these two cases. The radiation pattern of a long-wire antenna above a conducting plane consists of a number of lobes with the main lobe at small incidence angles with respect to the tip ($\approx 20°$), whereas the excitation of surface plasmons localized between a sphere (modeling the front part of the tip) and a conducting sample occurs in a single broad lobe peaking at 55°.[19]

Since difference-frequency signals were only detected with selected tips of very small diameter and since maximum signals were obtained at incidence angles of $\approx 20°$, it is concluded that for our experiments at a laser wavelength of 1.3 μm the radiation coupling conforms to antenna theory. Antenna theory can be used to calculate the voltage $\hat{V}_\omega$ between the tip and sample oscillating at the laser frequency ω (optical voltage). The result is given in[17]

$$\hat{V}_\omega = \frac{1}{\omega C R_a}\left(\frac{\eta I_0 \lambda l}{\pi^3 w_0^2}\right)^{1/2}, \tag{1}$$

where C is the tip–sample capacitance, R_a the antenna resistance, I_0 the laser intensity at the tunneling junction, l the effective antenna length, $\eta = 120\pi\Omega$, λ the laser wavelength, and $2w_0$ the beam diameter.

Attributing the generation of nonlinear tunneling current components to the nonlinear $I-V$ curve of the tunneling junction, we calculate a rectified current component I_r and a component $I_{\Delta\omega}$ at the difference frequency $\Delta\omega = \omega_1 - \omega_2$ (Ref. 17)

$$I_r = \frac{1}{4}\left.\frac{\partial^2 I}{\partial V^2}\right|_{V_b} (\hat{V}_{\omega_1}^2 + \hat{V}_{\omega_2}^2), \tag{2}$$

$$I_{\Delta\omega} = \frac{1}{4}\left.\frac{\partial^2 I}{\partial V^2}\right|_{V_b} \hat{V}_{\omega_1}\hat{V}_{\omega_2}, \tag{3}$$

where $\hat{V}_{\omega_1}$ and $\hat{V}_{\omega_2}$ are the optical voltages at the frequencies ω_1 and ω_2, and V_b is the bias voltage. The difference-frequency signal is emitted from the tip, which acts as a radiating dipole, and a power $P_{\Delta\omega}$ is received by an open waveguide with area A at a distance r and an angle θ:[17]

$$P_{\Delta\omega} = \frac{10.2\eta}{2^5\pi} A\left(\frac{l_{\Delta\omega}}{\lambda_{\Delta\omega}}\frac{\sin\theta}{r} I_{\Delta\omega}\right)^2. \tag{4}$$

The effective dipole length is $l_{\Delta\omega}$ and $\lambda_{\Delta\omega}$ is the wavelength of the difference-frequency signal.

This model successfully described difference-frequency generation in the STM with CO_2 laser radiation at 9.3 μm.[17] It is now applied to the measurements at 1.3 μm. The bias-voltage dependence of the difference-frequency signal in Eq. (3) is compared with experimental results presented in Figs. 3, 4, and 5. For this purpose Eqs. (3) and (4) are written in the following form:

$$P_{\Delta\omega}(V_b) = \alpha\left(\left.\frac{\partial^2 I}{\partial V^2}\right|_{V_b}\right)^2 P_{\omega_1} P_{\omega_2} + \gamma. \tag{5}$$

The fitting parameters α and γ describe the coupling and detection efficiencies, and the noise level, respectively. P_{ω_1} and P_{ω_2} are the laser powers.

For the calculation of $\partial^2 I/\partial V^2|_{V_b}$ the experimental $I-V$ curves for the different materials are approximated by fifth-degree polynomials [dotted curves in Figs. 3(a), 4(a), and 5(a)]. Fits of Eq. (5) to the different experimental curves are shown as dotted curves in Figs. 3(b), 4(b), and 5(b). The good agreement achieved for all three surface materials demonstrates that the nonlinearity of the static $I-V$ curve also determines difference-frequency generation at 1.3 μm.

A dependence on the wavelength of the laser radiation enters the model only in the description of the radiation coupling in Eq. (1). As the STM tips are nearly conical in shape, the effective antenna length in terms of the wavelength is expected to be constant. If all other parameters in Eq. (1) are wavelength independent, we obtain $\hat{V}_\omega \propto \lambda^2$. To test this hypothesis, we compare the optical voltages obtained from this experiment with values from an experiment with CO_2 laser radiation at 9.3 μm.[17]

The optical voltages are calculated by means of the experimental data from Figs. 3, 4, and 5. Combining Eqs. (3) and (4) and setting $\hat{V}_{\omega_1} = \hat{V}_{\omega_2} = \hat{V}_\omega$, $A = 2.3\,\mathrm{cm}^2$, $l_{\Delta\omega}/\lambda_{\Delta\omega} = 0.75$, $\sin\theta = 1$, $r = 20\,\mathrm{mm}$, we obtain $\hat{V}_\omega = 15.4$, 24.6, and 12.7 mV for Au, Ag, and HOPG, respectively. Since different laser powers and focal spot sizes were used in the experiments at 9.3 and 1.3 μm, we compare the values of $\hat{V}_\omega (P_L/w_0^2)^{-1}$. For the experiments at 1.3 μm the results are 0.96, 1.54, and 1.02 $\mathrm{mV\,cm^2\,kW^{-1}}$ for the three surface materials. For the experiment at 9.3 μm we use values from Ref. 17 and obtain 90 $\mathrm{mV\,cm^2\,kW^{-1}}$. With $\hat{V}_\omega \propto \lambda^2$, the optical voltage is expected to decrease by a factor of 50. Considering that the total conversion loss of difference-frequency generation in the STM is more than 130 dB, one can regard this deviation of 6 dB as small. We conclude that the antenna model for the radiation coupling describes the wavelength dependence rather well. In particular, we note that the radio frequency current is not found to increase at shorter wavelengths as expected from Ref. 12.

Equation (2) predicts rectification of the laser field. Besides the rectified current, however, the total laser-induced dc current usually also contains a thermal component. These two components may be distinguished using the simultaneous measurement of the laser-induced current and the mixing signal displayed in Fig. 6. The fact that a laser-induced current is still observable when the laser focus is moved by more than 30 μm from the tunneling junction clearly indicates the presence of a thermocurrent. Additional evidence emerges from a rough calculation of the rectified current using Eq. (2) together with an experimental value of the difference-frequency signal. An upper limit of the rectified current thus obtained turned out to be significantly smaller than the experimental value. We conclude that the dominant part of the laser-induced current found in the experiments is a thermocurrent.

Finally, we discuss the chemical contrast observed in the images of Figs. 7(b) and 8(b), which were recorded using the difference-frequency signal. This contrast was obtained by choosing the value of the bias voltage such that $\partial^2 I/\partial V^2|_{V_b}$ has a large difference for the two materials. An interesting feature is the deep valley seen on one of the islands when imaged with the difference-frequency signal [Fig. 8(b)]. This structure was reproduced on repeated scans. Since no other island showed a similar feature we attribute it to chemical contrast due to a molecular contamination. The spatial resolution of the difference-frequency signal in the images is limited by the pixel size to $\approx$30 nm [e.g., at the border of the island in Fig. 7(b)]. Atomic resolution is expected, as previously observed at a laser wavelength of 9.3 μm.[2] Further experiments in ultrahigh vacuum are necessary to demonstrate chemical contrast on an atomic scale.

CONCLUSIONS

We investigated the generation of gigahertz difference-frequency signals in the tunneling junction of the STM using diode-laser radiation at 1.3 μm. The experimental results are explained by a model which describes the radiation coupling by antenna theory and the mixing process by the nonlinearity of the $I-V$ characteristic of the STM. The measurements—when compared with previous results at a laser wavelength of 9.3 μm—show a decrease of the mixing signal power with the wavelength which is attributed to the decreasing efficiency of antenna coupling. Attempting to overcome this decrease by using larger incident laser powers leads to growing thermal instabilities of the tunneling junction (noise and drift). Spectroscopic applications of nonlinear signal generation in the STM in the near infrared and visible spectral ranges therefore call for investigation of other efficient methods of coupling laser radiation into the tunneling junction of the STM, e.g., excitation of localized surface plasmons.

[1] G. P. Kochanski, Phys. Rev. Lett. **62**, 2285 (1989).
[2] M. Völcker, W. Krieger, T. Suzuki, and H. Walther, J. Vac. Sci. Technol. B **9**, 541 (1991).
[3] M. Völcker, W. Krieger, and H. Walther, Phys. Rev. Lett. **66**, 1717 (1991).
[4] N. Kroo, J.-P. Thost, M. Völcker, W. Krieger, and H. Walther, Europhys. Lett. **15**, 289 (1991).
[5] W. Rohrbeck, E. Chilla, H.-J. Fröhlich, and J. Riedel, Appl. Phys. A: Solids Surf. **A52**, 344 (1991).
[6] W. Seifert, E. Gerner, M. Stachel, and K. Dransfeld, Ultramicroscopy **42–44**, 379 (1992).
[7] B. Michel, W. Mizutani, R. Schierle, A. Jarosch, W. Knop, H. Benedickter, W. Bächtold, and H. Rohrer, Rev. Sci. Instrum. **63**, 4080 (1992).
[8] S. J. Stranick and P. S. Weiss, Rev. Sci. Instrum. **64**, 1232 (1993).
[9] W. Krieger, T. Suzuki, M. Völcker, and H. Walther, Phys. Rev. B **41**, 10229 (1990).
[10] C. Baur, A. Rettenberger, K. Dransfeld, P. Leiderer, B. Koslowski, R. Möller, and P. Johansson, in *Photons and Local Probes*, edited by O. Marti and R. Möller (Kluwer, Dordrecht, 1995), p. 235.
[11] A. V. Bragas, S. M. Landi, J. A. Coy, and O. E. Martínez, J. Appl. Phys. **82**, 4153 (1997).
[12] M. J. Hagmann, J. Vac. Sci. Technol. B **14**, 838 (1996).
[13] K. Liu and M. G. Littman, Opt. Lett. **6**, 117 (1981).
[14] K. C. Harvey and C. J. Myatt, Opt. Lett. **16**, 910 (1991).
[15] L. Ricci, M. Weidemüller, T. Esslinger, A. Hemmerich, C. Zimmermann, V. Vuletic, W. König, and T. W. Hänsch, Opt. Commun. **117**, 541 (1995).
[16] M. Völcker, W. Krieger, and H. Walther, J. Appl. Phys. **74**, 5426 (1993).
[17] M. Völcker, W. Krieger, and H. Walther, J. Vac. Sci. Technol. B **12**, 2129 (1994).
[18] P. Johansson, R. Monreal, and P. Apell, Phys. Rev. B **42**, 9210 (1990).
[19] R. W. Rendell and D. J. Scalapino, Phys. Rev. B **24**, 3276 (1981).